Controllable synthesis of NaP zeolite and its application in calcium adsorption

Ibraheem O. Ali[1], Said M. El-Sheikh[2], Tarek M. Salama[1*], Mostafa F. Bakr[1] and Mohamed H. Fodial[1]

NaP zeolite particles were prepared through a template-free hydrothermal condition at 100ºC. Parameters like Na₂O/SiO₂ and SiO₂/Al₂O₃ molar ratios, gel aging time and aging temperature were investigated for regulating the crystallization of the final product. The samples at different synthesis stages were characterized with N₂ adsorption at −196ºC, field emission scanning electron microscopy (FE-SEM), temperature programmed desorption of ammonia adsorption, X-ray diffraction, thermogravimetric and differential scanning calorimetry analysis and Fourier transform infrared spectroscopy. The experimental results evidenced that a high ordering crystallinity of NaP zeolite was obtained at Na₂O/SiO₂ and SiO₂/Al₂O₃ molar ratios of 1.10 and 1.40, respectively, and a temperature of 100°C for 4 days of aging. FE-SEM image exhibited polycrystalline aggregates of NaP zeolite with crystallite sizes ranging up to 5.04 μm with cactus/cabbage like structures. The quantitative analysis of the total number of acid sites was found to increase as Na₂O increases. The NaP zeolite sample with a Na₂O/SiO₂ molar ratio of 1.13 exhibited a large fraction of the acid sites on its external surface, contrary to that synthesized with a relevant ratio of 1.10. The optimized NaP zeolite could be successfully bestowed with excellent sorption properties of Ca(II) in aqueous solution. The kinetic parameters for Ca(II) adsorption were thoroughly investigated.

INTRODUCTION

Zeolites are crystalline solids with an extending three dimensional network of aluminum and silicon tetrahedra linked by sharing of oxygen atoms [1,2]. The zeolite dimensional framework contains repeating cavities and channels, wherein monovalent and divalent cations, water and/or small molecules may reside inside. They are found to have particular applications in heterogeneous catalysis, petroleum refining, ion exchange, chemical separation, adsorption, host/guest chemistry, microelectronic devices, optics, and membranes [3,4]. Such applications of zeolites are strongly influenced by the particle morphology, pore size and architecture, and type of channels. In order to improve

functional performance of the different kinds of zeolites, many studies have been devoted to improving synthetic approaches to control crystal size, the size of the intracrystalline pore/channel system and morphology of zeolites [5,6].

Among various types of zeolites, NaP ($Na_6[(AlO_2)_6$ $(SiO_2)_{10}] \cdot 15H_2O$) is one of the most interesting structured zeolite with two sets of intersecting channels: 0.31 nm × 0.44 nm and 0.26 nm × 0.49 nm. According to International Zeolite Association (IZA), this structure is called "Gismondine" (GIS) framework topology [7,8]. NaP zeolite offers the greatest promise for gas separation applications due to its small pore size [9,10], and is also useful for removal of toxic and radioactive waste species like Cs, Sr, Ba, Pb, U, heavy metals, and ammonium from wastewater, seawater potassium extraction and formation of environmental friendly detergent [11,12].

NaP zeolite can be synthesized from various precursor materials and various methods. It can be synthesized from: (i) clay at a crystallization temperature of 85ºC [13], (ii) sodium silicate solution [14], and (iii) high silicon fly ash of coal combustion at 120ºC for 4 h [15]. Among them the most common methods used for the synthesis of NaP zeolite are the sol-gel technique, hydrothermal synthesis and microwave heating synthesis [1]. The NaP zeolite with different morphologies can offer many intriguing properties: places to store the guest molecules and to perform chemical reactions with selected-sized molecules. Thus, the NaP zeolite morphology and its important correlation with properties is the need of the recent research.

In this work, we attempted the template free hydrothermal synthesis of NaP under controlled conditions. Based on multiple paths that can be involved in the hydrothermal synthesis of NaP, optimization of crystallization conditions was adapted through variation of the following parameters: Na₂O/SiO₂ and SiO₂/Al₂O₃ molar ratios, aging time and aging temperature. The characteristics of the synthesized gels

[1] Department of Chemistry, Faculty of Science, Al-Azhar University, Nasr City 11884, Egypt
[2] Nanostructured Materials Lab, Advanced Materials Department, Central Metallurgical R&D Institute (CMRDI), Cairo 11421, Egypt
* Corresponding author (email: tm_salama@yahoo.com)

and products were studied by N_2 adsorption, field emission scanning electron microscopy (FE-SEM), temperature programmed desorption of ammonia adsorption (NH_3-TPD), X-ray diffraction (XRD), thermogravimetric (TG) and differential scanning calorimetry (DSC) analysis and Fourier transform infrared (FTIR) spectroscopy. The efficiency of the synthesized NaP zeolite was then tested for sorption of Ca(II) ions from aqueous solution on the optimum condition and the kinetic parameters were determined.

EXPERIMENTAL SECTION

Materials
All the chemicals used were of analytical grade and taken without further purification or modification: sodium aluminate (Al_2O_3 50–56 wt.%, Na_2O 40–45 wt.%, Sigma–Aldrich), silica fume (Sigma–Aldrich, fume 99.8%, melting point 1700°C) and sodium hydroxide pellets (99%, Merck). $CaCl_2$ solution (0.025 mol L^{-1}, BIOMED Diagnostics) and Arsenazo III (synonyms 2,7-bis(2-arsonohyenylazo)-1,8-dihydroxy-3, 6-naphthalene disulfonic acid or 2,2′-[1,8-dihydroxy-3,6-disulfo-2,7-naphthalene-bis(azo) dibenzenearsonic acid)], $C_{22}H_{18}As_2N_4O_{14}S_2$, molecular weight 776.37, 80%, Egyptian Company for Biotechnology) were used for the spectrophotometric determination of Ca(II).

Synthesis of NaP zeolite
The hydrogel was prepared by dissolving a specific amount of NaOH in 20 mL of distillate water and silica fume (2.5 g) in 40 mL of distillate H_2O with stirring. Then both of them were mixed together and stirred at room temperature and followed by heating at 80°C until a clear solution was obtained (solution A). A similar process was repeated by dissolving sodium aluminate (3.2 g) in 45 mL of distillate water, and a specific amount of NaOH in 20 mL of distillate water under stirring. Then both solutions were mixed together and stirred at ambient temperature until a clear solution was obtained (solution B). Solution B was added slowly to solution A with vigorous stirring. After the complete addition, the gel was formed and aged at room temperature for 30 min with vigorous stirring to get a homogeneous gel-mix, and then it was transferred to a stainless-steel autoclave (300 mL capacity). The sealed autoclave was placed in an air oven at 100°C for 4 days. The produced materials were then filtered, washed with water and dried at 100°C for 8 h.

Effect of Na₂O/SiO₂ molar ratio
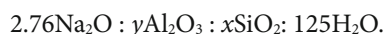The relative amounts (x) of Na_2O were varied with keeping the other component amounts constant as follows:

$$x Na_2O: 1.76Al_2O_3: y SiO_2: 125H_2O,$$
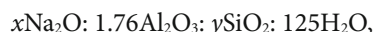
where $1.04 \leqslant x/y \leqslant 1.13$.

Effect of SiO₂/Al₂O₃ molar ratio
The $x SiO_2/y Al_2O_3$ ratios were varied between $1.10 \leqslant x/y \leqslant 5.70$ according to a gel composition:

$$2.76Na_2O : y Al_2O_3 : x SiO_2: 125H_2O.$$

The Na_2O/SiO_2 and H_2O/SiO_2 ratios in the gel route were kept constant at 1.10 and 16.0, respectively. The resulting gel was homogenized and transferred into the autoclave and allowed to react at 100°C for 4 days.

Effects of temperature and crystallization time
A batch of NaP zeolite was adopted at an initial molar composition of:

$$2.76\ Na_2O : 1.76Al_2O_3 : 2.5SiO_2 : 125H_2O.$$
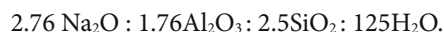
The temperature to induce crystallization of the NaP zeolite has been varied from 80 to 140°C to have comparable dimensions of different sizes and shapes, while the reaction period was fixed at 4 days. Experiments were also carried out in varied crystallization periods over 2–6 days during the synthesis of the same patch, while the temperature was fixed at 100°C.

Kinetic experiments
A measured amount (0.1 g) of the synthesized NaP zeolite was added to a measured amount (50 mL) of aqueous solution of Ca(II) of different initial concentrations (100–150 mg L^{-1}), and taken into 250 mL beakers at 27 ± 2°C and mixed on a magnetic stirrer at pH 7. 1.0 mL sample solution was withdrawn each time from the reaction mixture at a gap of fixed time interval, and filtered using Whatman filter paper to separate the adsorbent particles from the solution. The residual Ca(II) in sample solution was analyzed by UV-vis spectroscopy at 620 nm absorbance. The color intensity of a purple complex formed *in situ* from the reaction of Ca(II) and Arsenazo III is directly proportional to the adsorption capacity of the samples in the batch-reactor [16,17]. The amount of calcium adsorbed was calculated using the relation:

$$q_t = \frac{w_i - w_r}{m}, \tag{1}$$

where q_t is the adsorbed amount of calcium per unit mass of the adsorbent (mg g^{-1}) at any time (t), w_i and w_r the initial and residual amount (mg) of calcium added and

622

August 2015 | Vol.58 No.8

remained in solution, respectively, and *m* the mass of the adsorbent added (g).

Experimental techniques

Phase identification, purity, relative crystallinity and crystallite size of the products were analyzed with X-ray diffractometer (Panalytical X'Pert Pro, Netherland) using Cu-Kα as a source radiation and nickel filter at a scanning speed of 2° min^{-1} in the 2θ range from 4° to 70°. The crystallite size was calculated from XRD data by Scherrer equation.

Infrared spectra were recorded by FTIR spectrometer (JASCO 3600 Tokyo, Japan) using KBr tablets.

Brunauer-Emmett-Teller (BET) surface area analyzer (Nova 2000 series, Quanta chrome Instruments, UK) was used to determine the specific surface area (S_{BET}), pore volume and pore size distribution of the zeolite samples.

Thermal analysis (DSC-TG) of the NaP zeolite was performed at a heating rate of 10°C min^{-1} from 25 to 1000°C in an air flow using a Netzsch-Sta 409 C/CD instrument (Selb, Germany).

The number of acid sites and acid strength of the NaP zeolite were determined by means of temperature programmed desorption of NH$_3$ adsorption (NH$_3$-TPD) model BELCAT-B, with serial No. CAT–146. The samples were heated from room temperature up to 900°C at a heating rate of 10°C min^{-1} in a helium flow (200 cm^3 STP/min). The amount of NH$_3$ desorbed from the sample was monitored by a thermal conductivity detector (W-Re filament).

Size, particle morphology, and aggregation of the NaP zeolite were monitored by a FE-SEM (Quantafeg 250, Netherlands).

RESULTS AND DISCUSSION

Verified synthesis of zeolite NaP by XRD

Effect of Na$_2$O/SiO$_2$ molar ratio

Fig. 1a illustrates the XRD patterns of the synthesized NaP zeolite samples with different Na$_2$O/SiO$_2$ molar ratios, ranging from 1.04 to 1.13. The patterns of samples made with Na$_2$O/SiO$_2$ molar ratio varying from 1.04 to 1.07 exhibit crystalline peaks characteristic of both X- and P-type zeolites. When this ratio increased to 1.10, NaP zeolite was detected as the dominant phase (JCPDS No. 71-0962). Thus, a requisite quantity of sodium silicate is needed to tune the composition of the starting gel for crystallization of NaP zeolite. The significant increase in crystallinity of the produced NaP when the Na$_2$O/SiO$_2$ molar ratio is 1.10 could be discussed in terms of the role of OH$^-$ groups in increasing the nucleation rate of NaP zeolite, which properly accounts for the dissolution of the amorphous gel and

the formation and release of NaP zeolite heteronuclei at the gel-solution interface. This may lead to an effective acceleration of the crystal growth and shorten the induction period for the crystal growth of NaP zeolite [17–20]. Moreover, it was found that increasing the Na$_2$O/SiO$_2$ ratio to 1.13 in the synthesis gel resulted in the preservation of the NaP zeolite matrix, whose degree of crystallinity decreased slightly. This is due to the more density of negative charges involved in the framework structure.

Effect of SiO$_2$/Al$_2$O$_3$ molar ratio

It is well known that the catalytic activity increases with decreasing SiO$_2$/Al$_2$O$_3$ molar ratio in a zeolite. This is because as the aluminum content increases, the number of cations existing in the zeolite also increases to balance the negative charges of the zeolite framework. Hence, a series of NaP zeolite with different SiO$_2$/Al$_2$O$_3$ ratios from 1.10 to 5.70 was synthesized and the obtained diffractograms are depicted in Fig. 1b. For a first interacting gel with a SiO$_2$/Al$_2$O$_3$ molar ratio of 1.10, no appearance of NaP zeolite was observed, but instead, a mixture of zeolite Y and analcime was formed with a relatively low degree of crystallinity. With increasing SiO$_2$/Al$_2$O$_3$ ratio to 1.40, the product tended to favor the transformation to only NaP zeolite. A further increase in this ratio up to 2.30 brought about a significant decrease in the structural ordering of NaP zeolite without revealing any other competitive phases. At a much higher SiO$_2$/Al$_2$O$_3$ ratio of 5.70, the NaP zeolite phase completed disappeared, and the morphology of the gel became amorphous. Basically, these results agree well with those reported by Szostak [21] whereby the nucleation and crystallization rate of NaP zeolite can be enhanced as follows: (i) as the aluminum content decreases, (ii) with a SiO$_2$/Al$_2$O$_3$ ratio above 1.40 and (iii) the lesser the NaOH concentration, the higher the yield of the crystalline material obtained. Despite keeping the pH of each gel around 11.0, the total NaOH concentration of the gel varied depending on the content of NaAlO$_2$ added in order to set the SiO$_2$/Al$_2$O$_3$ ratio. Hence, a small amount of NaOH contained in a gel with a high molar ratio of SiO$_2$/Al$_2$O$_3$ would promote the formation of a high SiO$_2$/Al$_2$O$_3$ zeolite. This is due to the low relative solubility of the Al(III) ions with respect to the Si(IV) ions in alkaline NaOH solution.

Effect of hydrothermal treatment

The effect of hydrothermal aging in the range of 80–120°C on better control of NaP zeolite crystal growth was thoroughly investigated by XRD (Fig. 1c). The gel composition of the starting mixture was kept constant at SiO$_2$/Al$_2$O$_3$ and Na$_2$O/SiO$_2$ molar ratios of 1.40 and 1.10, respectively.
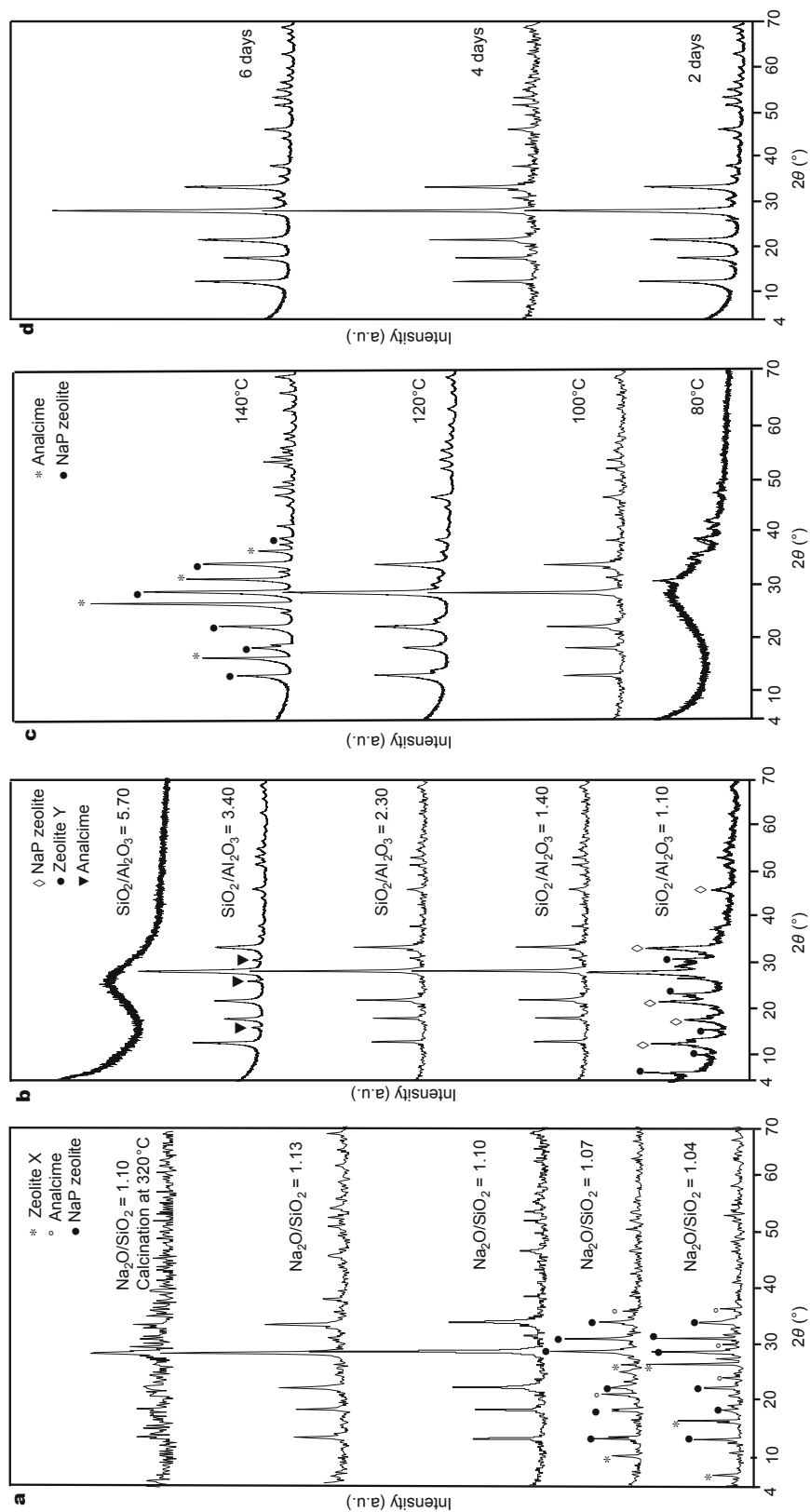
Figure 1 XRD patterns of zeolite NaP synthesized with different Na_2O/SiO_2 molar ratios (a), SiO_2/Al_2O_3 molar ratios (b), hydrothermal aging temperature (c) and aging time (d).

Initially, crystallization of NaP zeolite was insufficient at a temperature below 80°C, whereas the reflections reached maximum intensity at 100°C. Thus, a temperature of 100°C was considered to be optimum for getting the highest degree of NaP zeolite crystallinity. As the aging temperature increases to 120°C, the NaP pattern exhibits an overall reduction in the intensities of the reflections due to decreased crystal size. A further increase in temperature to 140°C results in crystal growth of the analcime parallel to NaP zeolite. In agreement with previous reports [22], the sequence of formation of the products with the increase in temperatures was in the direction: transient amorphous phase to NaP zeolite to analcime.

These results can be interpreted as due to the effect of supercritical concentration of components aluminate and silicate in the liquid phase of the mixture, generally a gel, which is the major controlling factor of zeolite formation [23]. Concentrations of these components are temperature-dependent, i.e. the concentration of the solution changes as the temperature changes. As the temperature increases over 100°C, the solubility of the aluminate and silicate species increases, causing a shift in the concentration of the liquid phase. As a consequence, an impurity of analcime in the phase of NaP zeolite would be produced at 140°C. Hence, if pure NaP zeolite has to be crystallized at high temperatures, lowering of the Na_2O/SiO_2 ratio is important in the starting mixture to attain relatively low alkalinity.

Effect of aging time

The effect of aging time on the hydrothermal crystallization of NaP zeolite under similar conditions, i.e. the SiO_2/Al_2O_3 and Na_2O/SiO_2 ratios in the final gel composition at 1.40 and 1.10, respectively, and a temperature of 100°C, is shown in Fig. 1d. A comparable crystallization behavior was achieved after hydrothermal aging the mixture over variable amounts of time. The XRD analysis reveals that the time required to achieve a maximum crystallization is 4 days since shorter or longer aging time than this period leads to the lower crystallinity of the zeolite particles. The gel aging do not influence the type of zeolite NaP formed. The primary effect of the gel aging for 4 days is the shortening of the induction period and the acceleration of the crystallization process. The increase in hydrothermal treatment time to 6 days implies a lower degree of crystallinity due to prolonged pressure induced amorphization.

FTIR spectra

Effect of Na_2O/SiO_2 molar ratio in the vibrational lattice frequencies and the crystallization field of NaP zeolite synthesized with Na_2O/SiO_2 = 1.13 and 1.10 molar ratios was

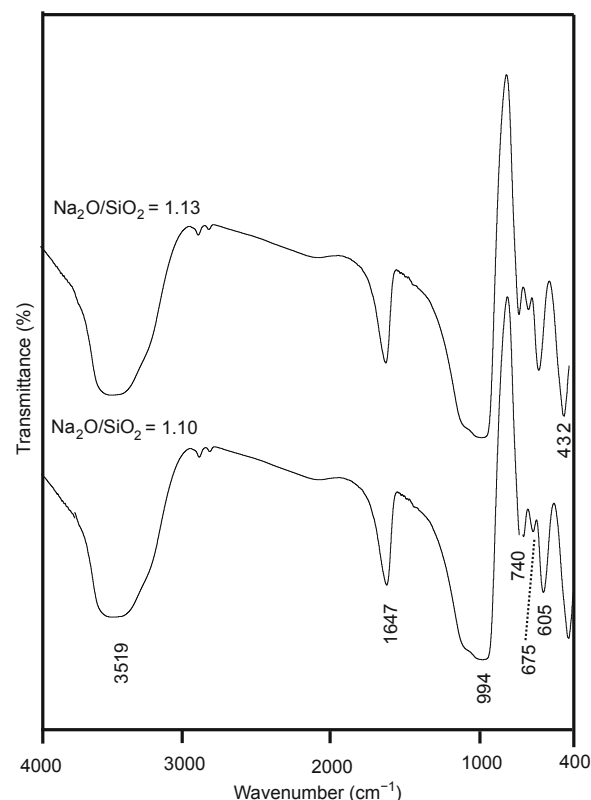**Figure 2** FTIR spectra of zeolite NaP prepared by using different Na_2O/SiO_2 molar ratios.

examined by FTIR (Fig. 2). The overall vibrations in the infrared spectra of both samples are typical of NaP zeolite [24]; the fundamental features at 994, 740, 675, 605 and 432 cm^{-1} were assigned generally to different vibrations of adjacent tetrahedra and framework atoms in the zeolite lattice [16,24,25]. The bands at about 994 and 432 cm^{-1} are due to internal vibrations of $(Si,Al)O_4$ tetrahedra of NaP zeolite which are insensitive to framework structure. These bands result from stretching and bending modes of the T–O (T=Si or Al) units [16], respectively. The shifting of the T–O band generally located around 1090–1040 cm^{-1} for aluminosilicates containing five-membered rings to lower frequencies (994 cm^{-1}), indicates zeolitization of the reacted slurry to NaP zeolite. Musyoka [26] observed a shift from 1053 to 1004 cm^{-1} and increased absorbance at 1004 cm^{-1} as the fly-ash/NaOH slurry was increasingly converted to NaP zeolite, with increasing hydrothermal treatment time at a temperature of 100°C.

The bands at 675 and 740 cm^{-1} are attributed to the symmetric stretch vibration of internal tetrahedra. The band at 605 cm^{-1} is due to vibrations related to doubling stretching framework structure [1]. The intensity of this band was

higher for sample made with the molar ratio of Na_2O/SiO_2 at 1.10 than its analogs at 1.13, which might suggest a higher ordered and well-defined structure for the former sample than the latter, incompatible with the XRD data. The IR band at 3519 cm^{-1} was assigned to hydrogen bonded Si–OH groups, while the band at 1647 cm^{-1} was ascribed to the bending vibration mode of residual H_2O molecules in the zeolite voids [27,28].

Thermal analysis

TG and DSC thermograms of the uncalcined samples of the synthesized NaP zeolite with Na_2O/SiO_2 molar ratios of 1.10 and 1.13 are depicted in Fig. 3. The shapes of these TG curves are all similar to the thermal behavior of the synthesized NaP zeolite [8]. These curves are characterized by weight losses of total mass 12.45 and 17.88 % of the former and latter samples, respectively. The first peak at 163°C in the profiles of both samples can be attributed to desorption of water molecules present on external and internal surfaces, that accompanied by weight losses of 8.0 and 15.0 wt.% for samples made with the Na_2O/SiO_2 ratio of 1.10 and 1.13, respectively. The second peak appeared at around 328°C with weight losses of 4.45% and 2.88% for the former and latter, respectively, corresponding to decomposition and removal of hydroxyl groups in the synthesized zeolites [28]. This means that the removal of hydroxyl groups in

the synthesized NaP zeolite increases with decreasing the Na_2O/SiO_2 molar ratio.

The DSC curves of the two samples showed two thermal effects (Fig. 4). The first endothermic effect with a maximum at 118°C was relevant to the release of water molecules from zeolite NaP. The exothermic effect at 328°C corresponds to the amorphous to crystalline transformation of NaP zeolite.

Related to this behavior, the TG curves of the two samples (Fig. 3), present endothermic peak at the same temperature due to condensation of surface silanol groups and/or removal of the chemically bound water [29]. The DSC effect at 328°C is more noticeable for the sample with Na_2O/SiO_2 = 1.10 than the one having Na_2O/SiO_2 = 1.13. This exothermic peak would be referred to partial decomposition of zeolite NaP made with the Na_2O/SiO_2 ratio of 1.10 into amorphous Al_2O_3- and SiO_2- like species on NaP where this sample experienced a disproportionate loss of crystallinity, in agreement with the XRD data of Fig. 1a. It should be noted that the synthetic P zeolites dominate the synthesis composition fields in the low temperature range (from 100 to 150°C). No further exothermic peaks related to phase transitions of the materials up to 1000°C were observed in the DSC curves of both samples to support their thermal stability in this temperature range.
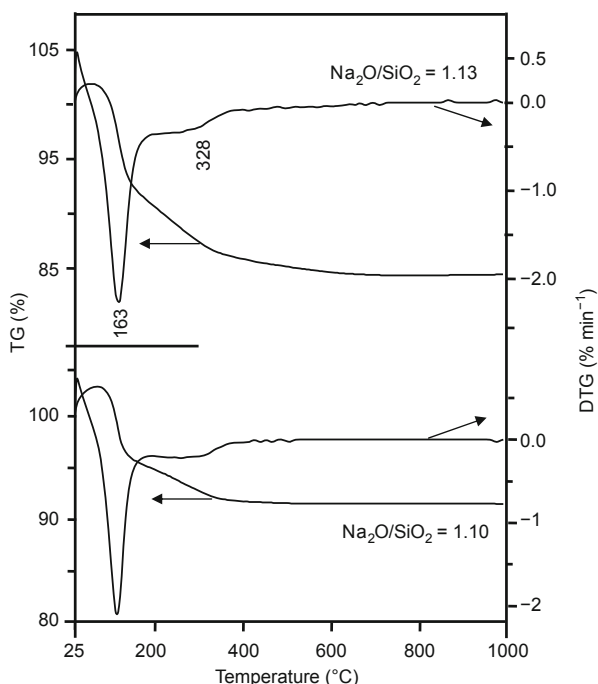

Figure 3 TGA curves of zeolite NaP prepared by using different Na_2O/SiO_2 molar ratios.

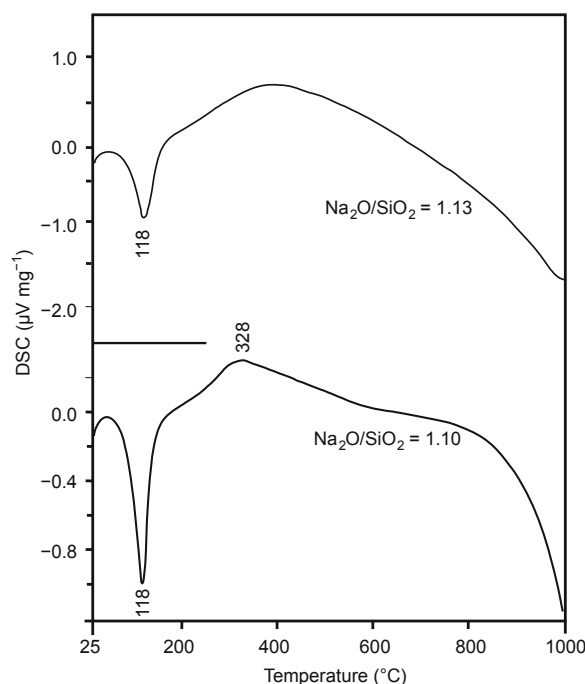**Figure 4** DSC curve of zeolite NaP prepared by using different Na_2O/SiO_2 molar ratios.

Morphology and crystal size

Particle size and morphological evaluation of the synthesized NaP samples with different Na_2O/SiO_2 (1.10 and 1.13) molar ratios were investigated by FE-SEM (Fig. 5). The difference in the Na_2O/SiO_2 ratio caused a slight difference in the average particle size of the samples. According to the FE-SEM image, the sample with a molar ratio Na_2O/SiO_2 of 1.10 exhibits cactus/cabbage-like morphology, which is characterized by polycrystals with an average size ranging up to 5.19 μm. The predominance of zeolite NaP as the final crystalline product is confirmed by the morphology development of such cactus/cabbage forms. These results are similar to those presented by Zubowa et al. [1], in which NaP zeolite was identified as pseudo-spherical forms constituted by small plates. When the Na_2O/SiO_2 ratio is 1.13, NaP zeolite was formed with a relatively smaller size, i.e. 5.04 μm. Likewise, the morphology of this sample is retained in cactus/cabbage forms. The enhanced nucleation might be responsible for the formation of smaller particle size in the sample with $Na_2O/SiO_2 = 1.13$.
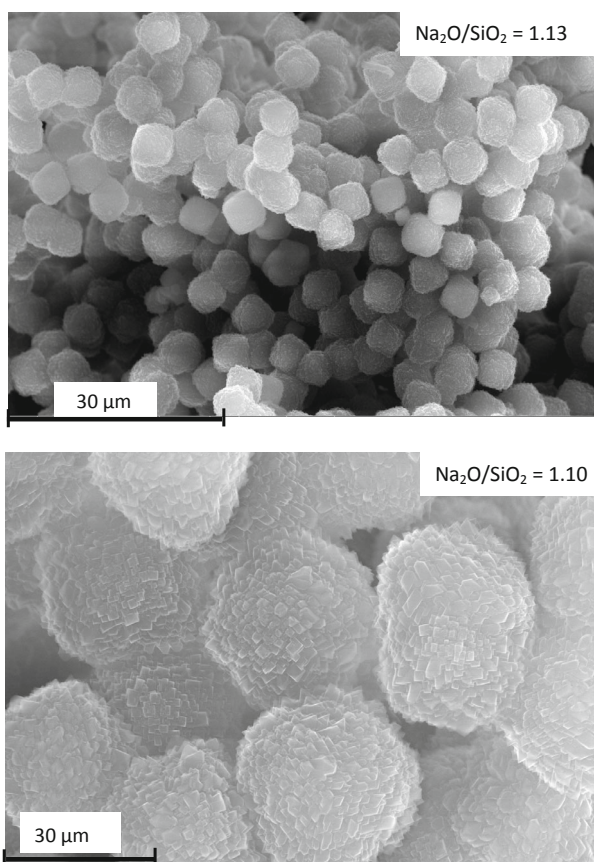
Temperature programmed desorption of NH_3

NH_3-TPD was used to measure the acid strength and the acid sites distribution on the surfaces of the samples with different Na_2O/SiO_2 molar ratios (Fig. 6). The NH_3-TPD profiles for both samples revealed two desorption peaks; a low temperature (LT) peak at 381°C and a high temperature (HT) peak at 442°C (Fig. 6). This leads to the assumption that at least two types of acid sites exist in both samples. The LT-peak represents intermediate strength, of acidic sites and assigned to the desorption of ammonia bound via hydrogen bonds to NH_4^+, i.e. $(NH_3)_nNH_4^+/Zeo^-$ adsorbate, and proton transport is assumed to follow a Grotthus-like mechanism [30,31]. It can be seen from the TPD profiles that the NaP sample with the higher Na_2O/SiO_2 molar ratio exhibited a large fraction of acid sites, contrary to that synthesized with the lower ratio.

The HT-peak may be attributed to the decomposition of the stoichiometric adsorption complexes, i.e. the NH_4^+/Zeo^- ion-pair complex, which formed by interaction with strong acidic Brønsted sites related to framework aluminum atoms. The majority of the structural Brønsted acid sites are located in the pores, only small amounts of Brønsted acid sites are on the outer surface of the NaP particles. The total number of acid sites initially increased from 1.89 to 4.43 mmol g^{-1} when Na_2O/SiO_2 molar ratio increased from 1.10 to 1.13, respectively. This can be explained by the removal of the extra framework debris in the former and thus generating mesopore-modified zeolite P, which
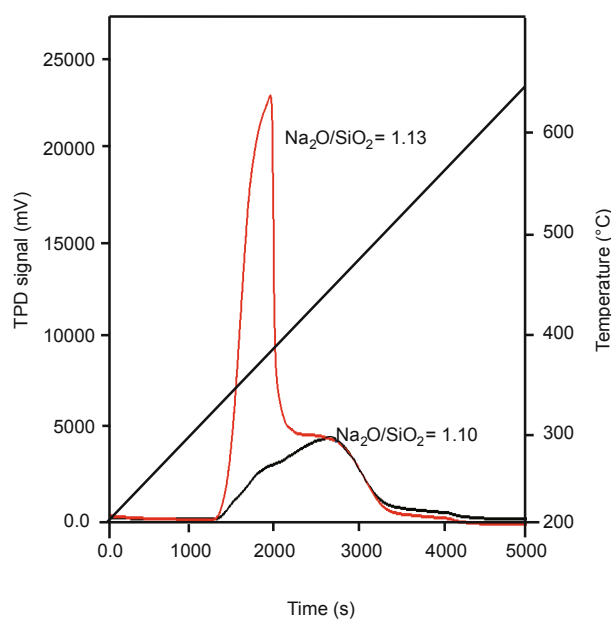

Figure 5 SEM images of zeolite NaP prepared by using different Na_2O/SiO_2 molar ratios.

Figure 6 NH_3-TPD of zeolite NaP prepared by using different Na_2O/SiO_2 molar ratios.

would best describe the higher total acidity of this sample. This is confirmed by the prevalence of wide pore volume (V_p^{wid}) and surface area of wide pores (S^{wid}) of this sample in which diffusion limitation was almost absent. Besides, the larger surface area of NaP zeolite made with the Na_2O/SiO_2 molar ratio of 1.13, as shown below, provides more sites for chemisorption of ammonia.

Surface texture

Surface characteristics of NaP zeolite samples prepared with Na_2O/SiO_2 =1.10 and 1.13 molar ratios were determined by N_2 adsorption/desorption experiments at −196°C. Both NaP zeolite samples show a type IV isotherm characteristic of solids with predominantly mesoporous channels [32] (Fig. 7). Although the validity of the BET model for highly microporous materials is questionable, the surface area derived from this model in the adapted pressure range $P/P°$ = 0.01–0.1 can still be used for comparative purposes [33] in Table 1. The specific surface areas were 6.16 and 13.63 m^2 g^{-1}, while pore volumes were 0.012 and 0.0022 cm^3 g^{-1} for samples made with Na_2O/SiO_2 = 1.10 and 1.13, respective-

ly. Thus, the latter sample exhibits a higher surface area and a lower pore volume, which is likely due to lower particle size of this sample as confirmed by XRD and FE-SEM. It can be seen that all surface area values were rather small, similar to those reported values in the literature, which could be attributed to the fact that NaP zeolite only had 8-membered rings in the structure [8,34].

Micropore-size distribution of both zeolite samples was calculated using HK-pore-size distributions method [35]. The HK method can be applied to differentiate micro pore size distribution maxima located close to each other in a physical mixture of two different zeolite materials as shown in Fig. 7 (inset). The HK profile of zeolite NaP with Na_2O/SiO_2 = 1.10 indicates the presence of micropores with a maximum pore size of 3.0 nm. Alternatively, the absence of a point of inflection in the high-resolution isotherm of the NaP sample with Na_2O/SiO_2 = 1.13 is a direct evidence for the absence of micropores in this sample.

Adsorption of Ca(II) in aqueous solution

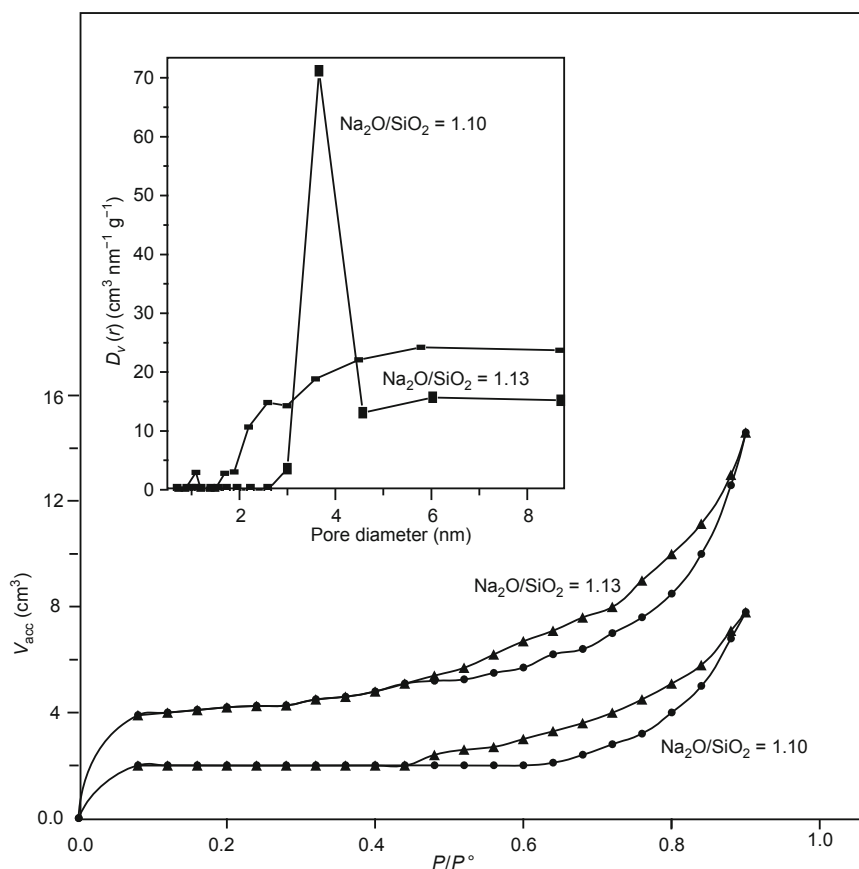The uptake profiles of 150 mg L^{-1} initial concentration of

Figure 7 N_2 adsorption-desorption isotherms of zeolite NaP prepared by using different Na_2O/SiO_2 molar ratios. The inset shows the HK-pore-size distributions of the NaP zeolites.
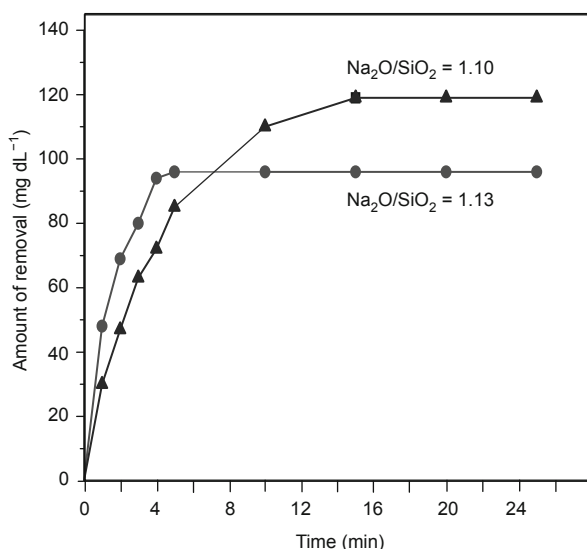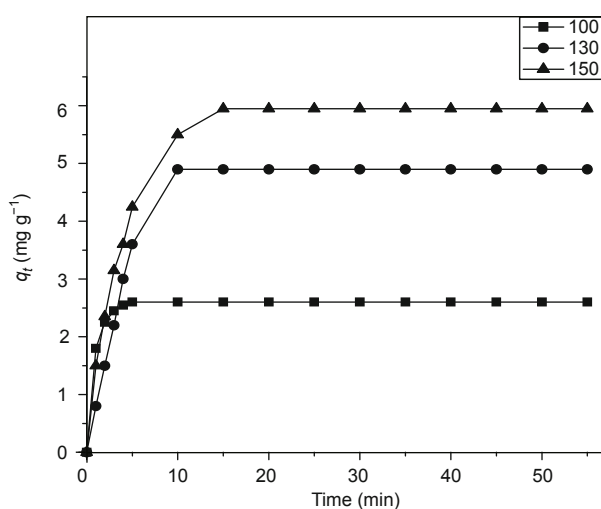
Table 1 Surface characteristics of zeolite P at different ratios of Na₂O/SiO₂ after thermal treatment at 200°C under reduced pressure of 10^{-5} Torr and nitrogen adsorption at −196°C

Sample	S_{BET} (m² g⁻¹)	S_t (m² g⁻¹)	S^{μ} (m² g⁻¹)	S^{wid} (m² g⁻¹)	S^{ext} (m² g⁻¹)	$\bar{r}$ (Å)	V_p^{total} (cm³ g⁻¹)	V_p^{μ} (cm³ g⁻¹)	V_p^{wid} (cm³ g⁻¹)
Na₂O/SiO₂=1.1	6.2	6.5	5.3	0.9	8.6	19.0	0.0120	0.0029	0.0091
Na₂O/SiO₂=1.13	13.3	13.7	6.9	6.4	6.8	19.1	0.0197	0.0037	0.016

Note: (S_{BET}) BET-surface area; (S_t) surface area derived from V_{1-t} plots; (S^{ext}) external surface area; (S^{μ}) surface area of micropores; (S^{wid}) surface area of wide pores; (V_p^{total}) total pore volum (V_p^{μ}) pore volume of micropores; ($\bar{r}$) mean pore radius.

Ca(II) against contact time show that the amount of Ca(II) adsorbed onto NaP increases as the Na₂O/SiO₂ ratio increasing from 1.10 to 1.13 at the early stage of adsorption, i.e. up to 5 min (Fig. 8). The uptake slows near to equilibrium beyond this period of the latter, though the former continued to adsorb Ca(II) ions up to 15 min. An inflection point in the sorption profiles was observed at 7.2 min. Initially a large number of vacant sorbent sites are available on zeolite NaP made with the Na₂O/SiO₂ molar ratio of 1.13, and there is a high concentration gradient between solution and solid interface, thus uptake was fast for the first 5 min, incompatible with the higher surface area of this sample. After this time, occupation of the remaining vacant surface sites is difficult due to repulsive forces between the solute molecules in the NaP zeolite (Na₂O/SiO₂ = 1.13) and bulk phase, and rate slows down. Between these two stages the rate of uptake is constant.

As can be seen from Fig. 9, the adsorption capacities of NaP zeolite with the Na₂O/SiO₂ molar ratio of 1.10, for

Figure 9 Effect of different concentration of Ca²⁺ from aqueous solution on adsorption to zeolite NaP.

Figure 8 Effect of contact time on the adsorption of Ca²⁺ from aqueous solution by zeolite NaP at the following conditions: temperature, 27°C; initial concentration, 150 mg/50mL; pH 7; adsorbent dosage, 0.1 g/50 mL.

Ca(II) ions were observed to increase with the increase of the initial Ca(II) ion concentrations, i.e. 100, 130 and 150 mg L⁻¹. Also, adsorption of Ca(II) increased with the contact time. This was attributed to the concentration gradient which can greatly contribute to the driving force for adsorption. High removal rates of Ca(II), within a few minutes, were observed at the beginning of adsorption process because of the great number of sites available for the sorption uptake. The maximum percentage removal of Ca(II) has been found to be 79.3% for 150 mg L⁻¹ initial Ca(II) concentration, until the equilibrium condition was achieved. The equilibrium began firstly, after 5 min at a lower concentration of Ca(II), i.e. 100 mg L⁻¹; then delayed by 10 and 15 min at 130 and 150 mg L⁻¹, respectively. It is argued that this performance should be similar to the migration volume for "free" vacancies in the framework structure of the NaP zeolite.

Adsorption isotherm analysis

The Freundlich and Langmuir isotherms are important for analysis and design of the sorption systems and to fit the

experimental data. The Langmuir equation was applied to the sorption equilibrium as follows:

$$\frac{C_e}{q_e} = \frac{C_e}{q_{max}} + \frac{1}{q_{max}K_L}, \qquad (2)$$

where q_e is the amount of Ca(II) adsorbed at equilibrium (mmol g^{-1}), C_e is the equilibrium concentration of the solution (mg L^{-1}), q_{max} is the maximum adsorption capacity (mmol g^{-1}) and K_L is a Langmuir constant related to the binding energy of the sorption system (L g^{-1}).

A straight line is obtained by plotting C_e/q_e vs. C_e, where K_L and q_{max} could be estimated from the intercept and slope, respectively (Table 2). It can be concluded, from the values of R^2 and the maximum monolayer coverage capacity (q_m) obtained from Langmuir isotherms on both samples, that there is strong positive evidence that the sorption of Ca(II) onto NaP zeolite (Na$_2$O/SiO$_2$ = 1.10) has a better agreement with the Langmuir sorption model than the other sample (Na$_2$O/SiO$_2$ = 1.13).

The Langmuir isotherm can also be expressed in terms of a dimensionless constant separation factor (R_L) which is given by the following equation [36]:

$$R_L = \frac{1}{(1 + K_L C_0)}, \qquad (3)$$

where R_L is a dimensionless separation factor indicating the shape of the isotherm, K_L is the Langmuir constant and C_0 is the initial Ca(II) concentration. The Langmuir isotherm is favorable when $R_L < 1$, which is in a good agreement with the calculated data, i.e. $R_L = 0.0008$ and 0.0005 for the NaP zeolite samples made with Na$_2$O/SiO$_2$ of 1.10 and 1.13, respectively, which indicate the favorable adsorption of Ca(II) onto both samples.

Instead, the Freundlich isotherm model assumes the heterogeneous surfaces of adsorption isotherm. The Freundlich equation is commonly given as follows [37]:

$$\ln q_e = \ln K_F + \frac{1}{n}\ln C_e, \qquad (4)$$

where K_F (L g^{-1}) is the Freundlich constant, whose value indicates the adsorption capacity of the adsorbent, and $1/n$

is the Freundlich coefficient. By plotting $\ln(q_e)$ vs. $\ln(C_e)$, a straight line was obtained, where the values of n and K_F can be determined from the slope and intercept, respectively (Table 2). The results indicate that the $1/n$ value was less than unity for both zeolites, suggesting more facile adsorption of Ca(II) ions. Further, the R^2 for the NaP zeolite with the Na$_2$O/SiO$_2$ molar ratio of 1.13 was higher than the corresponding of 1.10, thus the experimental data of the former presents a better fit to the Freundlich isotherm.

The adsorption values were compared with the literature data in Table 2. Our results are in the range of cited values in the literature, where for instance Qin et al. [38,39] found that zeolite P had a maximum adsorption capacity for Ca^{2+} of 92.5 mg g^{-1}. Meanwhile, Kabwadza et al. [40] reported a higher adsorption value, i.e. 250 mg g^{-1}.

Kinetic analysis

The kinetics of adsorption of Ca(II) onto both NaP zeolite samples were inspected through the pseudo-first-order and pseudo-second-order kinetic models. The linearized-integral form of the pseudo-first-order model [41] is expressed as

$$\log(q_e - q_t) = \log q_e - \frac{K_1 t}{2.303}, \qquad (5)$$

where q_e and q_t are the amounts (mg g^{-1}) of Ca(II) adsorbed onto NaP at equilibrium time and at any instant of time t, respectively. K_1 (min^{-1}) is the pseudo-first-order reaction rate constant which is evaluated by plotting $\log(q_e - q_t)$ vs. t. The parameter values of the kinetic models at various Ca(II) concentrations are listed in Table 2. Here, the R^2 values are relatively low for both samples which implys that the adsorption does not fit well to the pseudo-first-order model.

Instead, the pseudo-second-order model assumed that the rate of a chemical exchange reaction occurring on the adsorbent surface may describe the number of adsorption sites available for the exchange as expressed by [42]

$$\frac{t}{q_t} = \frac{1}{k_2 q_e^2} + \frac{t}{q_e}, \qquad (6)$$

Table 2 Kinetic parameters for Ca^{2+} adsorption on Ca-selective zeolite

Sample NaP	Langmuir				Freundlich			Pseudo 1st order		Pseudo 2nd order			Ref.
	q_m (mg g^{-1})	K_L (L mg^{-1})	R_L	R^2	K_F (mg g^{-1})	$1/n$	R^2	K_1 (min^{-1})	R^2	k_2 (g mg^{-1} min^{-1})	q_e (mg g^{-1})	R^2	
Na$_2$O/SiO$_2$ = 1.10	170	82.3	0.0008	0.998	3.874	0.156	0.855	0.360	0.843	0.063	0.219	0.978	Our work
Na$_2$O/SiO$_2$ = 1.13	147	132.5	0.0005	0.983	3.820	0.143	0.945	0.884	0.902	0.076	0.059	0.993	
Literature work	250	/	0.0027	0.96	4.0	0.588	0.94	/	/	/	/	/	[40]
	92.50	2.06	0.247	0.994	42.20	0.136	0.905	0.305	0.997	0.0073	0.975	0.999	[38,39]

where q_e (mg g^{-1}) is the quantity of Ca(II) adsorbed at equilibrium state, q_t adsorbent at time t, and k_2 (g mg^{-1} min^{-1}) is the pseudo-second-order reaction rate constant. By plotting t/q_t against t, we can obtain k_2 and q_e from the intercept and the slope, respectively. Here, the results obtained from the analysis of the Ca(II) adsorption on both samples correspond to $0.99 \leqslant R^2 < 1.00$. Hence, the obtained experimental kinetic data fit well with pseudo-second-order kinetic equation. The higher the Na$_2$O/SiO$_2$ molar ratio, the higher pseudo-second-order rate constant was observed. The reason comes from the effects of total basicity in the higher Na$_2$O/SiO$_2$ sample which may drive the Ca(II) adsorption to the zeolite surface faster. The higher Na$_2$O/SiO$_2$ ratio (1.13) has been proven to allow the crystalline aluminosilicate to be formed due to the role of stabilization, thus have more sites for the NH$_3$ adsorption via NH$_3$-TPD data. From the TPD results, the LT peak at 381°C for NaP with Na$_2$O/SiO$_2$ (1.13) reveals the weakly molecular bonding state of NH$_3$, and most likely corresponds to Freundlich adsorption. The HT peak at 442°C indicates the dissociation of the NH$_4^+$/Zeo$^-$ ion-pair complex, which plausibly thought to be due to NH$_3$ molecules bind to the strong acid sites located on zeolite surface. In this case, one can use this peak to represent the Langmuir adsorption.

CONCLUSIONS

The NaP zeolite was successfully synthesized via a free template hydrothermal route with well-defined size and morphology control. The optimized combination of many factors such as inorganic components in the starting hydrogel can decisively control the synthesis of NaP zeolite especially the NaO$_2$/SiO$_2$ molar ratio. The physicochemical characterization showed that the optimized product in the synthesis of zeolite NaP was obtained at the Na$_2$O/SiO$_2$ molar ratio of 1.10–1.13, and aging temperature and time of 100°C and 4 days, respectively. The Na(I) cation was found to play an important structure-directing role in enhancing the nucleation and thermal stability of NaP zeolite crystals. Therefore, no exothermic peaks related to phase transitions of the materials up to 1000°C were observed in the DSC curves. The NH$_3$-TPD profile revealed two desorption ammonia peaks at 381 and 442°C for both samples. The latter with the Na$_2$O/SiO$_2$ molar ratio of 1.13 has been found to possess a much higher population of acid sites on its external surface at 381°C. The Langmuir isotherm model provided the best fit for a sample made with the Na$_2$O/SiO$_2$ ratio of 1.10, whereas Freundlich isotherm model successfully applied to that of 1.13. Kinetic parameters showed

that the adsorption of Ca(II) onto zeolite NaP for both samples was described best by pseudo-second order model confirming that this sorbent was chemically controlled. This happened with a shorter time required for reaching the equilibrium.

1 Zubowa HL, Kosslick H, Mueller D, *et al*. Crystallization of phase-pure zeolite NaP from MCM-22-type gel compositions under microwave radiation. Micropor Mesopor Mater, 2008, 109: 542–548

2 Meftah M, Oueslati W, Amara ABH. Synthesis process of zeolite P using a poorly crystallized kaolinite. Phys Procedia, 2009, 2: 1081–1086

3 Cao JL, Liu XW, Fu R, Tan ZY. Magnetic P zeolites: synthesis, characterization and the behavior in potassium extraction from seawater. Sep Purif Technol, 2008, 63: 92–100

4 Huang Y, Dong D, Yao J, *et al*. *In situ* crystallization of macroporous monoliths with hollow nap zeolite structure. Chem Mater, 2010, 22: 5271–5278

5 Wang F, Wu D, He S, *et al*. Property characterization of NaP1 zeolite from coal fly ash by hydrothermal synthesis. J Mater Eng, 2005, 8: 47

6 Dua YC, Shia SL, Daib HX. Water-bathing synthesis of high-surface-area zeolite P from diatomite. Particuology, 2011, 9: 174–178

7 Dong JH, Lin YS. *In situ* synthesis of p-type zeolite membranes on porous α-alumina supports. Ind Eng Chem Res, 1998, 37: 2404–2409

8 Breck D. Zeolite Molecular Sieves. New York: John Wiley & Sons, 1974

9 Brown GT, Osinga TJ, Parkington MJ. Steel AT. Zeolite P, process for its preparation and its use in detergent compositions. EP Patent 0384070, 1995

10 Kakansson L, Falth L, Hansen S. Structure of a high-silica variety of zeolite NaP. Acta Cryst C, 1990, 46: 1363–1364

11 Atkins M, Glasser FP, Jack JJ. Zeolite P in cements: its potential for immobilizing toxic and radioactive waste species. Waste Manage, 1995, 15: 127–135

12 Nery JG, Mascarenhas YP, Cheetham AK. A study of the highly crystalline, low-silica, fully hydrated zeolite P ion exchanged with (Mn^{2+}, Cd^{2+}, Pb^{2+}, Sr^{2+}, Ba^{2+}) cations. Micropor Mesopor Mater, 2003, 57: 229–248

13 Sathupunya M, Gulari E, Wongkasemjit S. ANA and GIS zeolite synthesis directly from alumatrane and silatrane by sol-gel process and microwave technique. J Eur Ceram Soc, 2002, 22: 2305–2314

14 Murayama N, Yamamoto H, Shibata J. Mechanism of zeolite synthesis from coal fly ash by alkali hydrothermal reaction. Int J Miner Proc, 2002, 64: 1–17

15 Kazemian H, Naghdali Z, Kashani TG, Farhadi F. Conversion of high silicon fly ash to Na-P1 zeolite: alkaline fusion followed by hydrothermal crystallization. Adv Powder Technol, 2010, 21: 279–283

16 Mullins LJ, Tiffert T, Vassort G, Whittembury J. The effects of internal Na$^+$ and H$^+$ and of external Ca^{+2} and membrane potential on Ca entry in squid axons. J Physiol, 1983, 338: 295–319

17 Vassort G, Whittembury J, Mulins LJ. Increases in internal Ca^{2+} and decreases internal H$^+$ are induced by general anesthetics in squid axons. J Biophys Soc, 1986, 50: 11–19

18 Kim SD, Noh SH, Park JW, Kim WJ. Organic-free synthesis of ZSM-5 with narrow crystal size distribution using two-step temperature process. Micropor Mesopor Mater, 2006, 92: 181–188

19 Kim SD, Noh S H, Seong KH, Jung Kim W. Compositional and ki-

netic study on the rapid crystallization of ZSM-5 in the absence of organic template under stirring. Micropor Mesopor Mater, 2004, 72: 185–192

20 Ali IO, Hassan AM, Shaaban SM, Soliman KS. Synthesis and characterization of ZSM-5 zeolite from rice husk ash and their adsorption of Pb^{2+} onto unmodified and surfactant-modified zeolite. Sep Purif Technol, 2011, 83: 38–44

21 Szostak R. Molecular Sieves: Principles of Synthesis and Identification, Van Nostrand Reinhold catalysis series. Amsterdam: Springer Netherlands, 1998, 123: 5

22 Barrer RM, White EAD. The hydrothermal chemistry of silicates. Part II. Synthetic crystalline sodium aluminosilicates. J chem Soc. 1952, 1561–1571

23 Zhdanov SP. Some problems of zeolite crystallization. Adv Chem Ser, 1971, 101: 20–43

24 Albert BR, Cheetham AK, Stuart JA, Adams CJ. Investigations on P zeolites: synthesis, characterisation, and structure of highly crystalline low-silica NaP. Micropor Mesopor Mater, 1998, 21: 133–142

25 Zhiping H, Xiangyu X, Zhi L, et al. Synthesis of zeolite NaP with controllable morphologies. Micropor Mesopor Mater, 2012, 158: 137–140

26 Musyoka NM. Hydrothermal Synthesis and Optimisation of Zeolite Na-P1 from South African Coal Fly Ash. MSc thesis, Cape Town: University of the Western Cape, 2009

27 Ali IO, Thabet MS, El-Nasser KS, Hassan AM, Salama TM. Synthesis of nanosized ZSM-5 zeolite from rice straw using lignin as a template: surface-modified zeolite with quaternary ammonium cation for removal of chromium from aqueous solution. Micropor Mesopor Mater, 2012, 160: 97–105

28 Pal P, Das JK, Das N, Bandyopadhyay S. Synthesis of NaP zeolite at room temperature and short crystallization time by sonochemical method. Ultrasonics Sonochemis, 2013, 20: 314–321

29 Mohamed MM, Salama TM, Othman I, Abd Ellah I. Synthesis of high silica mordenite nanocrystals using o-phenylenediamine, Micropor Mesopor Mater. 2005, 84: 84–96

30 Katada N, Niwa M. Analysis of acidic properties of zeolitic and non-zeolitic solid acid catalysts using temperature-programmed desorption of ammonia. Catal Surv Asia, 2004, 8: 161–170

31 Rodríguez-González L, Rodríguez-Castellón E, Jiménez-López A, Simon U. Correlation of TPD and impedance measurements on the desorption of NH$_3$ from zeolite H-ZSM-5. Solid State Ion, 2008, 179: 1968–1973

32 Li X, Li B, Xu J. Synthesis and characterization of transitional metal-rich zeolite M-MFI (M = Fe, Co, Ni, Cu) with regular mesoporous channels. Colloid Surf A Physicochem Eng, 2013, 434: 287–295

33 Rouquerol F, Rouquerol J, Sing KSW, et al. (eds.). Handbook of Porous Materials, Vol. 1. Weinhiem: Wiley-VCH, 2002, 250

34 Zhiping H, Xiangyu X, Lü Z, et al. Synthesis of zeolite NaP with controllable morphologies. Micropor Mesopor Mater, 2012, 158: 137–140

35 Horvath G, Kawazoe K. Method for the calculation of effective pore size distribution in molecular sieve carbon. J Chem Eng Jpn, 1983, 16: 470–475

36 Webber TW, Chakkravorti RK. Pore and solid diffusion models for fixed-bed dsorbers. AIChE J, 1974, 20: 228–238

37 Freundlish HMF. Over the adsorption in solution. J Phys Chem, 1906, 57: 385-470

38 Qin C, Wang R, Ma W. Adsorption kinetic studies of calcium ions onto Ca-selective zeolite. Desalination, 2010, 259: 156–160

39 Qin C, Wang R, Ma W. Characteristics of calcium adsorption by Ca-selectivity zeolite in fixed-pH and in a range of pH. Chem Eng J, 2010, 156: 540–545

40 Kabwadza-Corner P, Munthali MW, Johan E, Matsue N. Comparative study of copper adsorptivity and selectivity toward zeolites. Amer J Anal Chem, 2014, 5: 395–405

41 Lagergren S. About the theory of so-called adsorption of soluble substances. K Svenska Vetenskapsakad Handlingar Band, 1898, 24: 1–39

42 Singh KK, Rastogi R, Hasan SH. Removal of Cr(VI) from wastewater using rice bran. J Colloid Interface Sci, 2005, 290: 61–68

Conflict of interest The authors declare that they have no conflict of interest.

Ibraheem O. Ali received his BSc and PhD degrees from Chemistry Department, Faculty of Science, Al-Azhar University in the field of inorganic chemistry. Recently, he has been promoted as a professor of material science and catalysis at the Faculty of Science, Al-Azhar University. His research interests include zeolite synthesis, materials design and surface modification.

Tarek M. Salama was born in Cairo, Egypt. He received his BSc and PhD degrees from Al-Azhar University (Cairo, Egypt) and Hokkaido University (Sapporo, Japan), respectively. He then obtained a postdoctoral position in prof. Hediki Hattori's earth and environmental science lab in 1991. He joined the Catalysis Research Center (CRC), Hokkaido University, Japan (1993–1997) as a research professor where he worked with prof. Masaru Ichikawa on gold/NaY and gold/ZSM-5 systems for chemical, environmental and other industrial applications. As a professor of material science at the Faculty of Science, Al-Azhar University, his research interests focus on controlled synthesis of zeolites, assembly of inorganic nanomaterials and tailored design of carbon-based materials like nano ferrites loaded into nano graphene oxide and graphene.

中文摘要　　本文通过无模板水热法在100°C条件下制备了NaP沸石分子筛, 并研究了Na_2O/SiO_2和SiO_2/Al_2O_3摩尔比、凝胶老化时间和老化温度等参数, 以调节最终产品的结晶度. 不同合成阶段的样品, 用−196°C氮吸附、场发射扫描电子显微镜(FE-SEM)、氨程序升温脱附、X-射线衍射、热重和差示扫描量热分析以及傅里叶变换红外光谱法进行了表征. 实验结果表明, 在Na_2O/SiO_2和SiO_2/Al_2O_3摩尔比分别为1.10和1.40, 100°C温度下老化4天, 可以获得高度有序结晶化的NaP分子筛. FE-SEM图像显示NaP分子筛的多晶聚集体晶粒尺寸可达5.04 μm, 具有仙人掌/卷心菜样结构. 定量分析发现酸位点总数随Na_2O的增加而增加, Na_2O/SiO_2摩尔比为1.13的NaP沸石样品与1.10摩尔比合成的样品相比, 在外表面上具有大量的酸位点. 优化后的NaP分子筛在水溶液中具有优异的钙离子吸附性能, 本文对钙离子吸附动力学参数进行了详细研究.